International Journal of Pharmaceutics 670 (2025) 125116

Contents lists available at ScienceDirect

International Journal of Pharmaceutics

journal homepage: www.elsevier.com/locate/ijpharm

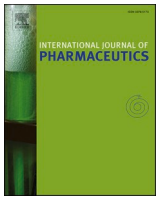

Selective laser sintering for printing bilayer tablets

Laura Andrade Junqueira [a], Atabak Ghanizadeh Tabriz [a], Vivek Garg [b], Siva Satyanarayana Kolipaka [c], Ho-Wah Hui [d], Nathan Boersen [d], Sandra Roberts [d], John Jones [e], Dennis Douroumis [a,c,*]

[a] Delta Pharmaceutics Ltd., Chatham, Kent ME4 4TB, UK
[b] Wolfson Centre for Bulk Solids Handling Technology, Faculty of Engineering & Science, University of Greenwich, Central Avenue, Chatham ME4 4TB, UK
[c] Centre for Research Innovation (CRI), University of Greenwich, Chatham ME4 4TB, UK
[d] Drug Product Development, Bristol Myers Squibb, 556 Morris Avenue, Summit, NJ 07901, USA
[e] Bristol Myers Squibb, Reeds Lane, Moreton, Wirral, UK

ARTICLE INFO

Keywords:
3D printing
Selective laser sintering
Bilayer tablets
Oral solid dosage forms

ABSTRACT

In this study Selective Laser Sintering (SLS) was used to produce bilayer tablets containing rosuvastatin and acetylsalicylic acid. Initially, monolithic tablets of each drug were manufactured using different laser intensities in order to identify their impact on the tablet's dissolution, friability and hardness. After the optimization, the final bilayer tablet was fabricated using a new method, that allowed the printing using different powder blends. For that, a 3D-printed casing was employed to maintain the compartments of the tablet in the correct position during the printing process. The results demonstrated that the increased laser intensities led to denser inner cores, enhanced hardness, decreased friability, and slower drug release. Moreover, the new method was able to produce bilayer tablets completely aligned, showing a minor impact on dissolution when the two compartments were printed together in a single tablet. The work demonstrated the feasibility of using SLS in the production of multi-material drug delivery systems.

1. Introduction

Three-dimensional printing, also known as additive manufacturing, represents a transformative technology where objects are constructed layer by layer, guided by a digital 3D design (Alzahrani et al., 2022). Currently, 3D printing has seen widespread applications across various industries, covering the production of items such as models, toys, food, high-end art, fashion pieces, and components for aircraft (Jakus and Introduction, 2019). In the healthcare sector, 3D printing has been used for generating anatomical prototypes for surgical planning (Mallon and Farnan, 2021) and medical education (Youman et al., 2021); development of prosthetics (Van Der Stelt et al., 2021) and medical devices (He et al., 2022); and bioprinting involving viable cells, biomaterials, and biological molecules (Alonzo et al., 2022). Notably, 3D printing holds great promise in the pharmaceutical field, particularly in the manufacturing of medicines. The approval of the first 3D-printed medicine, Spritam® by Aprecia Pharmaceuticals, in 2015 marked a significant milestone, sparking increased interest from both the academic community and the pharmaceutical industry in the 3D printing of medicines (Pereira et al., 2020).

3D printing facilitates the personalization of medicines enabling the production of small batches with customizable features including dosage, release profile, and physical attributes (e.g. size, shape, and color) (Beer et al., 2021). This capability has the potential to revolutionize the pharmaceutical sector, shifting from the traditional mass manufacturing of one-size-fits-all tablets to tailored dosage forms that align with the specific clinical needs of individual patients (Sandler and Preis, 2016). Moreover, this technology opens new avenues in the development of drug delivery systems by allowing the production of medicines with unique characteristics (Patel et al., 2021; Osouli-Bostanabad and Adibkia, 2018). Lastly, 3D printing empowers decentralized manufacturing of medicines, responding to on-demand needs at various points of care (Abdella et al., 2021; Araújo et al., 2019).

Over the years, a variety of 3D printing techniques have been established and successfully applied in the production of medicines in diverse dosage forms. The primary technologies employed for this

* Corresponding author at: Pharmaceutical Technology and Process Engineering, Chatham Maritime, Centre for Research Innovation, University of Greenwich, Chatham, Kent ME4 4TB, UK.
E-mail address: D.Douroumis@gre.ac.uk (D. Douroumis).

https://doi.org/10.1016/j.ijpharm.2024.125116
Received 1 October 2024; Received in revised form 17 December 2024; Accepted 19 December 2024
Available online 20 December 2024

purpose include Fused Deposition Modelling (FDM) (Scoutaris et al., 2018; Fu et al., 2018; Eleftheriadis et al., 2021; Melocchi et al., 2021), Inkjet printing (Cader et al., 2019; Uddin et al., 2015; Junqueira et al., 2022), Semi-solid extrusion (Yan et al., 2020; Tagami et al., 2021; Liu et al., 2020), and Stereolithography (Triacca et al., 2022; Karakurt et al., 2020). Although there are some investigations on Selective laser sintering (SLS) for pharmaceutical applications, it has not been fully exploited yet. In SLS, a focused, high-powered energy source, such as a laser, is employed to sinter or melt a bed of powder, fusing the particles together and resulting in the solidification of the material (Charoo et al., 2020). SLS is a solvent-free method, requiring little to no pre or post-processing, such as extrusion, post-curing, or complex removal of support. Consequently, it is typically a one-step process, characterized by reduced costs, simplicity, shorter processing times, and minimal material losses compared to other printing technologies. Moreover, SLS is user-friendly with a compact footprint. These advantages collectively make SLS an appealing printing technology for point-of-care applications, where efficiency and simplicity are crucial. Nevertheless, some issues such as powder de-dusting, the need for filtration systems, and occupational health risks due to large amounts of powders can cause some drawbacks on SLS applications for drug products.

To date, SLS has demonstrated remarkable flexibility, allowing for the fabrication of a diverse range of medicines. These include orally disintegrating tablets (Fina et al., 2018), controlled release devices (Leong et al., 2006), floating drug delivery systems (Kulinowski et al., 2022), amorphous solid dispersions (Davis et al., 2021), and personalized tablets (Tabriz et al., 2023). Additionally, extensive research has delved into the impact of printing parameters and formulation variables on the final product (Barakh Ali et al., 2019; Mohamed et al., 2020; Salmoria et al., 2013). However, there is a lack of knowledge regarding the fabrication of polypills or bilayer tablets using SLS. The study by Awad et al. (2019) is the only one reporting the use of SLS in the production of dual miniprintelets (1 and 2 mm in diameter) containing paracetamol and ibuprofen, achieving either immediate or sustained release based on the polymer employed (Awad et al., 2019).

The utilization of multiple medications to manage complex diseases such as cancer and cardiovascular disorders is an increasingly employed therapeutic strategy. Traditionally, each active pharmaceutical ingredient (API) is administered in an isolated dosage form (Khaled et al., 2015). However, this approach may result in patient confusion and higher rates of non-adherence to therapy (Robles-Martinez et al., 2019). In response to these challenges, the combination of different APIs in a single tablet, featuring appropriate release profiles and doses, emerges as an appealing alternative (Khaled et al., 2015; Robles-Martinez et al., 2019). In this context, the objective of this study was to investigate the use of SLS for the fabrication of bilayer tablets loaded with rosuvastatin and acetylsalicylic acid aiming at the management of heart conditions. The impact of laser intensity on dissolution, friability and hardness was evaluated; and the printing was optimized to achieve the bilayer tablets.

2. Materials and methods

2.1. Materials

Rosuvastatin calcium (RSV) (Mesochem Technology Ltd, China) and acetylsalicylic acid (AAS) (TCI Europe N.V., Belgium) were selected as model drugs. Kollidon VA 64 (VA64) was kindly donated by BASF (Germany) and Hypromellose acetate succinate (HMPCAS-LMP) (AQOAT® AS-LMP) by Shin-Etsu Chemical Co (Japan) were selected as the model polymers.

2.2. Blend preparation

Two physical mixtures (PM) were prepared, one composed of VA64 with AAS (72/28 wt%) and the second of HMPCAS-LMP with RSV (90/10 wt%). The powders were sieved using a 500 μm-mesh and the physical blends were mixed using a turbula shaker-mixer (Glen Mills T2F Shaker/Mixer, USA) at 72 rpm for 10 min to ensure blend homogeneity.

2.3. Thermal gravimetric analysis (TGA)

Thermal stability of the bulk materials and PMs were investigated using TGA (TGA Q5000 Thermal instruments, Crawley, UK). Approximately 5 mg of both samples were accurately weighed and then placed into standard 40 μL aluminum pans. The samples underwent heating from 25 °C to 400 °C at a rate of 10 °C/min. Subsequently, the raw data extracted was analyzed using TA Universal Analysis software (Universal Analysis 2000, version 4.5A, TA instruments, UK).

2.4. Differential scanning calorimetry (DSC)

DSC (Mettler-Toledo 823e, Switzerland) was employed to assess the thermal characteristics of both the bulk materials and the PMs. About 5 mg of each material was carefully placed into a 40 μL aluminum pan and promptly crimped. The samples underwent heating from 25 °C to 180 °C at a rate of 10 °C/min. The resulting DSC thermograms were then analyzed using STARe Excellence Thermal Analysis software V18 (Mettler Toledo, Greifensee, Switzerland).

2.5. Powder blend characterisation

2.5.1. Particle size distribution

Laser diffraction was used to measure the particle size distribution of the powder blends, employing a Mastersizer 3000 (Malvern Panalytical, Malvern, UK). Sample dispersion was achieved through a dry dispersion unit set at 2.2 bar air pressure with a 50 % feed rate to ensure consistent particle flow into the measurement area. Each measurement was conducted in triplicate and data analysis was carried out using Mie Theory. An averaged result from all measurements was used for the study.

2.5.2. Particle morphology

SEM (Hitachi SU8030, Tokyo, Japan) was employed to examine the particle morphology of both powder blends. The samples were dispersed on an aluminum stub coated with carbon adhesive tape (Agar Scientific, Stansted, UK). Images were acquired using an electron beam accelerating voltage of 1 KV and a magnification of 30 × .

2.5.3. Flowability test (bulk and tapped density)

The Carr's Index (I) of the 3D printing blend was determined by assessing the tapped and bulk densities of the powder. Initially, the bulk density was measured using a 250 mL graduated cylinder. Subsequently, the powder underwent 1250 taps using a tapped density tester (Copley, JVi Series—Model JV 200i, UK) in accordance with USP2 standards. The Carr's Index of the blend was then calculated using Equation (1):

$$I = \frac{\boldsymbol{P_T} - \boldsymbol{P_B}}{P_T} \times 100 \quad (1)$$

where I is the Carr's index, P_T the tapped density, P_B the bulk density.

2.6. Design and 3D printing of tablets

The tablets designs were created via 3D computer-aided design (CAD) software [SolidWorks software V.31 (Dassault Systems, Waltham, MA, USA)] and converted into stl files. Next, the stl files were transferred to the slicing software (Slic3r 1.2.9) for the generation of the G-codes file, which is readable by the printer. The tablets were printed using a SnowWhite SLS printer (SHAREBOT, Nibionno, Italy) equipped with a 14 W CO2 laser. Initially, monolithic tablets of each formulation were printed using different laser intensities. Then, based on the in vitro dissolution results, the best condition was selected to print the bilayer

Table 1
Tablet features and processing parameters for AAS and RSV blends.

	AAS	RSV
Weight (mg)	250	200
Thickness (mm)	2.0; 2.2; 2.4	1.8, 2.0, 2.2
Laser power (%)	20, 25, 35, 45	16, 20, 25
Environment temperature (°C)	60	95
Wait time (s)	600	600
Layer height (mm)	0.2	0.2
Powder feed layer (mm)	0.55	0.50
Scanning speed (pps)	8000	4000

tablet. The tablets presented a disk geometry and the diameter was set as 12 mm. The thickness was variable, depending on the laser intensity, to achieve a constant weight. The tablet features and processing parameters for each bled are shown in Table 1.

2.7. Physical characterization of the tablets

To physically characterize the tablets, hardness, friability and weight variation tests were conducted. The Schleuniger 5Y Tablet hardness tester (Pharmatron, Thun, Switzerland) was employed to measure the force required to break six 3D-printed tablets. Additionally, the friability was based on USP method with modification, where the 3D-printed tablets (n = 20, with total weight of approximately 4–5 g) were weighed and carefully placed into an EF-2L fibrillatory apparatus (ELECTROLAB, India), which rotated at 25 rpm for 4 min. Subsequently, the tablets were re-weighed, and the relative weight loss was calculated using Equation (2).

$$F = ((W_i - W_f)/W_i) \times 100 \quad (2)$$

where F is the friability, Wi is the initial weight of the tablets, and Wf is the tablet weight after the test. For the weight variation, ten 3D-printed tablets were carefully weighed using an analytical scale (XSR Analytical Balance, Mettler Toledo, Greifensee, Switzerland). The average weight and percentage of weight variation were then calculated.

2.8. X-ray powder diffraction (XRPD)

XRPD analysis was conducted to determine the physical states of the

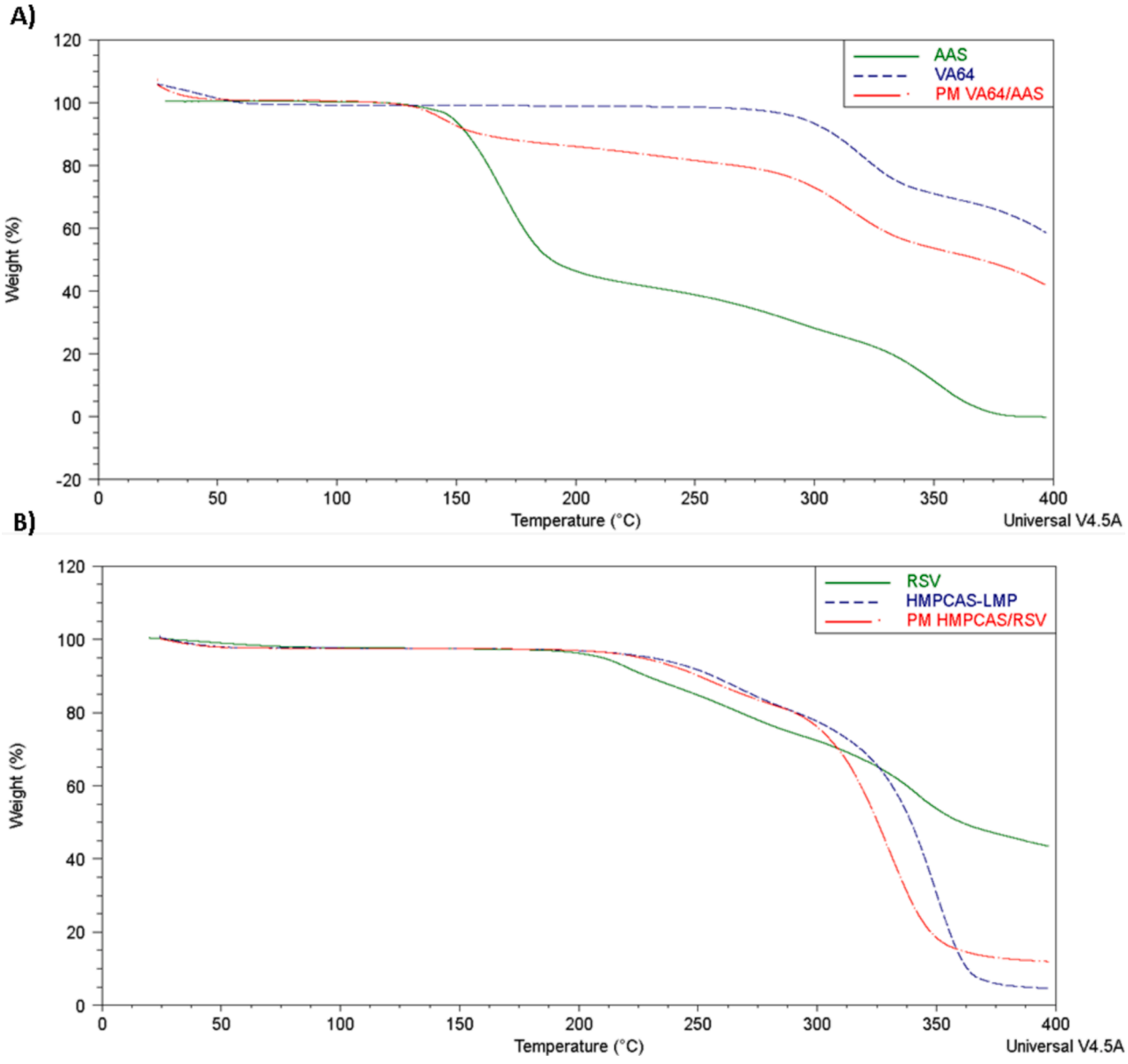

Fig. 1. TGA thermograms of A) AAS, VA64 and PM VA64/AAS. B) RSV, HMPCAS-LMP and PM HMPCAS/RSV.

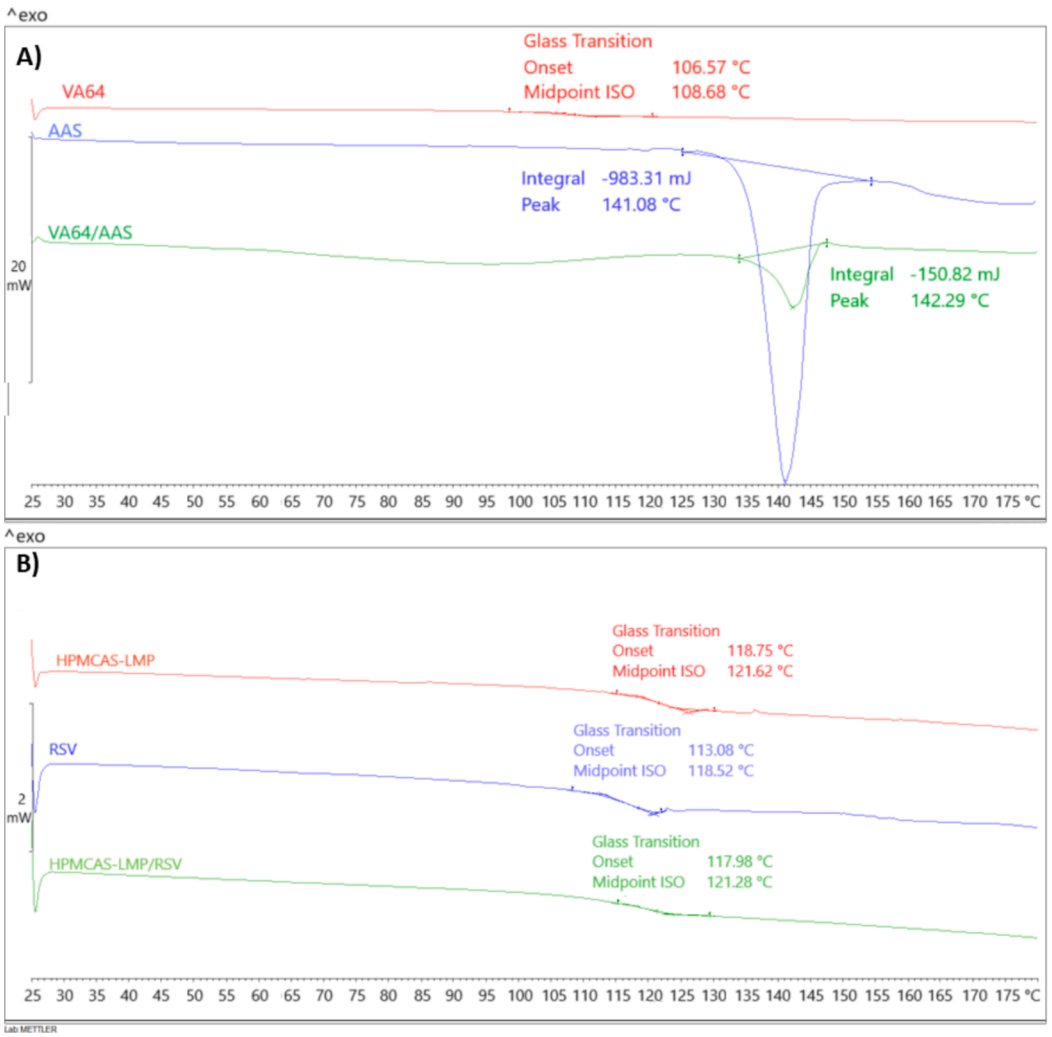

Fig. 2. DSC thermograms of A) AAS, VA64 and PM VA64/AAS. B) RSV, HMPCAS-LMP and PM HMPCAS/RSV.

bulk materials and the APIs within the monolithic tablets post-3D printing. The data were acquired using a D8 Advance X-ray diffractometer (Bruker AXS, Karlsruhe, Germany) equipped with a LynxEye silicon strip position-sensitive detector and parallel beam optics. The diffractometer operated in transmission geometry mode, employing Cu Kα radiation at 40 kV and 40 mA, respectively. Control of the instrument was managed through XRPD commander software (Version 2.6.1, Bruker AXS, Germany), with data analysis conducted using EVA software (version 5.2.0.3, Bruker AXS, Germany). Data collection spanned from 5 to 60° 2θ, with a step size of 0.04° and a counting time of 0.2 s per step.

2.9. Scanning electron microscopy (SEM)

SEM analysis was performed to evaluate the internal microstructures of the 3D-printed monolithic tablets and the impact of laser intensity on tablet porosity and permeability. A vertical section of the 3D-printed monolithic tablets were affixed to an aluminium stub using conductive carbon adhesive tape (Agar Scientific, Stansted, UK). A Hitachi SU8030 instrument (Tokyo, Japan) was employed with accelerating voltage of 1 kV and magnifications of 30 × .

2.10. In vitro dissolution and high-performance liquid chromatography (HPLC) analysis

In vitro dissolution studies of the 3D-printed tablets were performed according to USP guidelines (USP 41–NF 36 and 40 NF 35) with modifications. A USP II paddle apparatus (Varian 705 DS, USA) was used with 900 mL of dissolution medium at 37 ± 1 °C and a paddle speed of 50 rpm. The monolithic tablets were evaluated in citrate buffer for 1 h (pH = 4.5 for AAS and 6.6 for RSV). The bilayer tablets were subjected to dissolution testing for 1 h in citrate buffer at pH 4.5 and then were transferred for 1 h in citrate buffer at pH 6.6. All dissolution studies were carried out in triplicate. At specific time intervals, aliquots of 3 mL were collected and filtrated in a 0.45 μm filter before the analysis. The same volume of fresh media was added to each vessel to maintain a constant volume of dissolution media during the release study. The samples were then evaluated using HPLC to quantify the APIs.

The analysis was performed using an Agilent 1200 series HPLC system equipped with a gradient elution system, autosampler, C8 (5 μm, 250x4.6 mm) column for RSV, C18 (4.0-mm × 30-cm) column for AAS and UV detector at 280 nm (RSV and AAS). The mobile phase comprised of a) 2 g/L of sodium 1-heptanesulfonate in a mixture of acetonitrile and water (15:85) for AAS and b) 0.1 mol/L formic acid – methanol (25:75, v/v) pumped at flow rates of 2.0 and 1.0 mL/min respectively. Calibration curves were prepared using references for all drugs at concentrations of 10, 20, 30, 40, and 50 μg/mL ($R^2 = 0.999$).

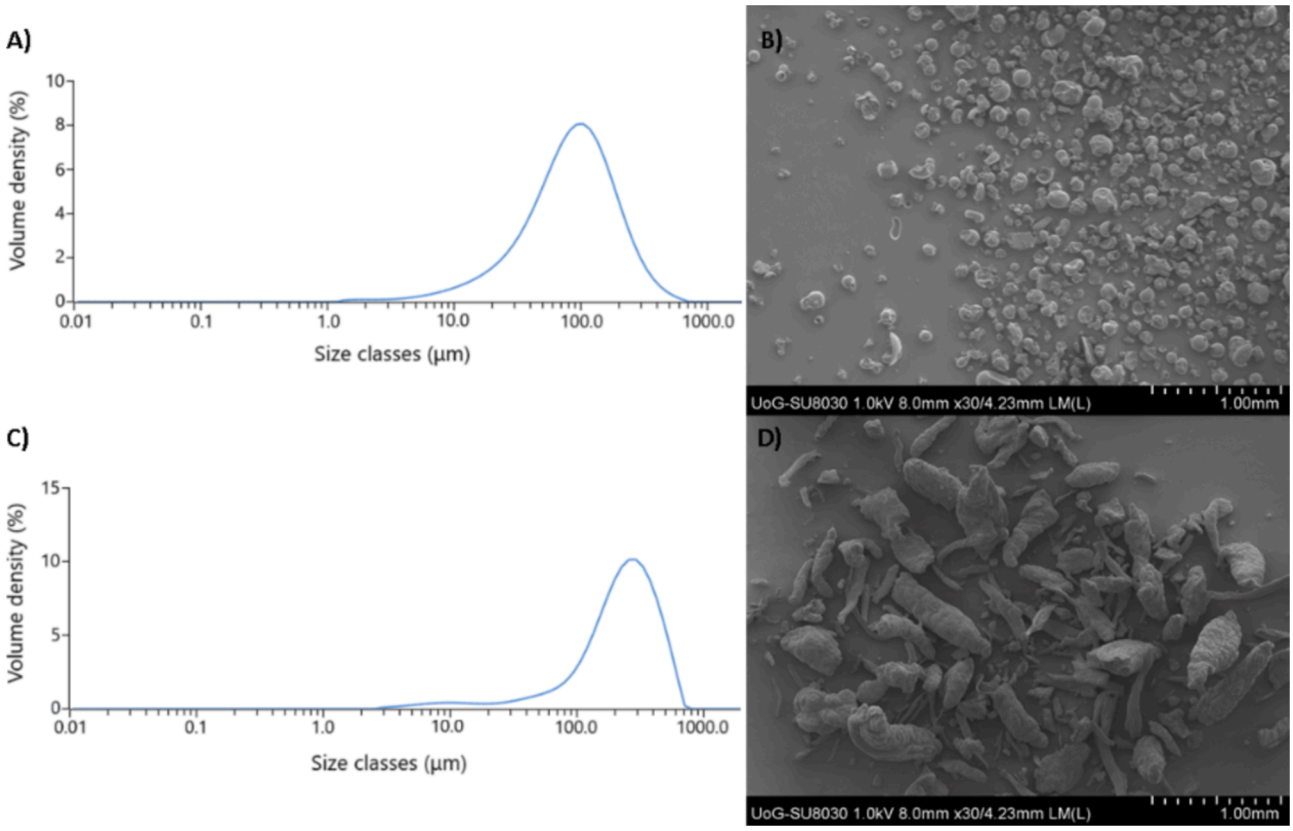

Fig. 3. Characterisation of the powders utilized for 3D printing. AAS/VA64 PM: A) particle size distribution, B) SEM image (30 × magnification). RSV/HPMCAS-LMP PM: C) particle size distribution, D) SEM image (30 × magnification).

Fig. 4. Monolithic 3D-printed tablets produced using SLS with different laser intensities. A) Formulation of VA64/AAS printed at 20, 25, 30, and 35% of laser intensity. B) Formulation of HMPCAS-LMP/RSV printed at printed at 16, 20 and 25%.

3. Results and discussion

3.1. Rational for drug and dose strength

The tablets in this study were designed for the treatment and prevention of cardiovascular conditions with a dose of 70 mg for AAS and 20 mg for RSV. For this purpose, clinical guidelines recommend a low dose of AAS, typically 75–100 mg daily (Arnett et al., 2019), and a dose range of 5–40 mg for RSV (Chou, R.; Cantor, A.; Dana, T.; Wagner, J.; Ahmed, A.; Fu, R.; Ferencik, M. Statin Use for the Primary Prevention of Cardiovascular Disease in Adults: A Systematic Review for the U.S. Preventive Services Task Force. Rockville (MD): Agency for Healthcare Research and Quality (US);, 2022). It is quite common that for combination pharmacotherapy the recommended doses are below the standard active dose (Yusuf et al., 2014). For example, certain cases, such as for elderly patients, those with lower body weight, or individuals with specific health conditions (e.g., chronic kidney or liver disease), lower doses of aspirin may be necessary, demonstrating the flexibility and potential applicability of this approach. Furthermore, 3D printing offers a unique advantage in the personalization of therapy, including customizable dosages that may be required in specific situations.

Table 2
Physical properties of the AAS and RSV 3D-printed tablets including hardness, friability, and weight variation.

Tablet	Hardness (N)	Friability (%)	Tablet weight (mg, weight variation %)
AAS 20	15 ± 1.8	16.4 ± 1.1	251. 2 (<2 %)
AAS 25	57 ± 1.5	6.2 ± 0.5	257.6 (<2 %)
AAS 35	152 ± 1.3	0.8 ± 0.01	255.4 (<1 %)
AAS 45	150 ± 1.1	0.6 ± 0.01	252.3 (<1 %)
RSV 16	12 ± 2.0	26.1 ± 2.6	208.5 (<2%)
RSV 20	64 ± 1.4	8.5 ± 1.2	206.3 (<1%)
RSV 25	110 ± 1.1	1.4 ± 0.01	203.0 (<1%)

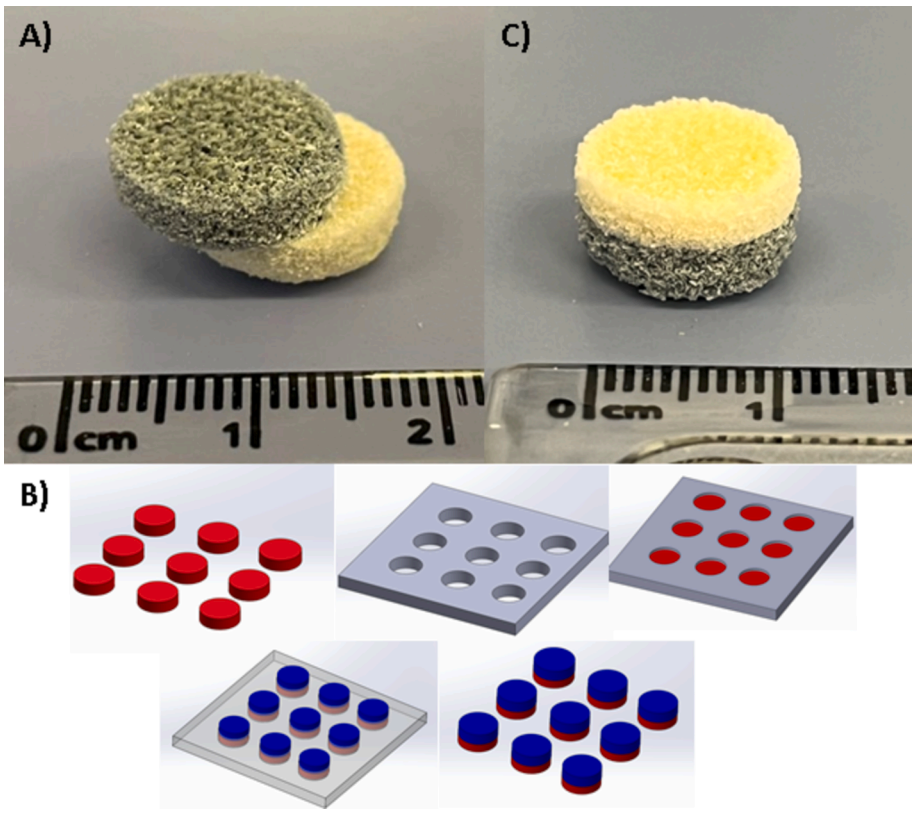

Fig. 5. Optimization of bilayer tablets using SLS. A) Image of the misaligned bilayer tablet fabricated without casing. B) Schematic representation of the new technique to produce bilayer tablets using a casing. C) Image of the aligned bilayer tablet fabricated with casing.

Fig. 6. Optical image of the 3D-printed bilayer tablet containing RSV and AAS produced by SLS.

Table 3
Physical properties of the bilayer's tablets including hardness, friability, and weight variation.

Tablet	Hardness (N)	Friability (%)	Tablet weight (mg, weight variation %)
Bilayer (35–20)	95 ± 1.2	1.8 ± 0.01	455. 7 (< 2 %)
Bilayer (45–25)	120 ± 1.1	0.9 ± 0.01	453.9 (<1 %)

3.2. Thermal analysis

TGA experiments were conducted to assess the thermal stability of the bulk materials and physical blends. Given the high temperatures experienced by powder particles during SLS printing, determining their thermal stability is crucial for establishing the optimal printing temperature and preventing degradation. As illustrated in Fig. 1A, VA64 exhibited an initial mass loss of 6 % due to moisture content and remained thermally stable up to 275 °C, after which rapid mass loss occurred due to polymer degradation.

AAS showed two distinct mass loss steps: the first between 130–235 °C accounting for approximately 60 % mass loss, and the second between 235–385 °C reaching 100 % mass loss. The physical mixture of VA64 and AAS exhibited initial water loss similar to VA64, followed by two mass loss steps between 120–210 °C (approximately 20 % mass loss) and 250–400 °C, achieving a roughly 60 % weight loss. Fig. 1B illustrates that HMPCAS-LMP remains stable up to 230 °C, beyond which it undergoes significant thermal degradation, with around 70 % mass loss at 350 °C. Conversely, RSV exhibited initial water loss followed by thermal stability up to 200 °C, after which degradation occurred. Finally, the physical mixture of HMPCAS-LMP and RSV began degrading around 230 °C.

As illustrated in Fig. 2, AAS exhibited a melting endothermic peak at 141.08 °C, while VA64 displayed a glass transition at 108.68 °C. In the VA64/AAS physical blend, the AAS melting peak shifted to 142.29 °C, and is not possible to observe the VA64 glass transition. Bulk RSV and HMPCAS-LMP presented glass transitions at 118.52 °C and 121.62 °C, respectively. Moreover, a glass transition was observed at 121.28 °C for the HMPCAS-LMP/RSV blend. Based on these values, the environmental temperatures for SLS-3D printing were set at 60 °C and 95 °C, staying below the glass transition and melting points of all materials. The precise selection of temperature is crucial for printing; otherwise, premature melting of the blend before laser radiation could negatively impact the process.

3.3. Powder blend characterisation

In the SLS process, powder flow plays a crucial role, directly

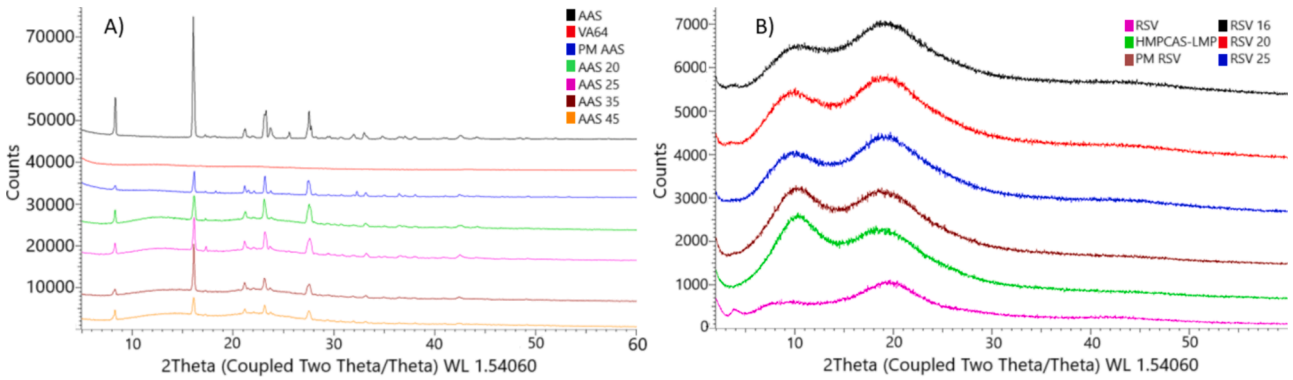

Fig. 7. XRD diffractograms of bulk materials, PMs and 3D-printed tablets at different laser intensities. A) AAS formulations; B) RSV formulations.

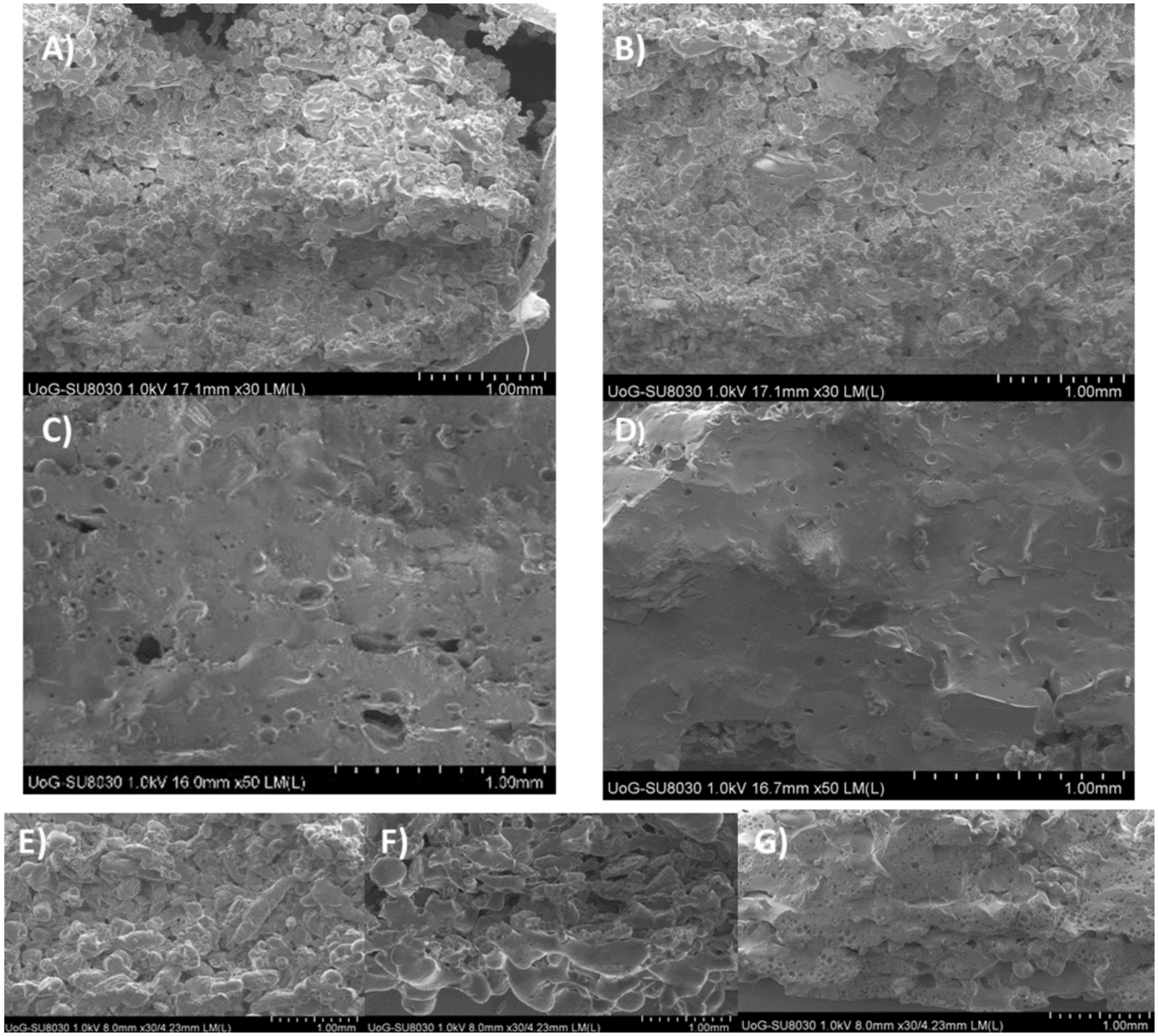

Fig. 8. SEM images of cross-sections of the 3D-printed tablets. AAS tablets printed at: A) 20%; B) 25%; C) 30% and D) 35% laser intensities. RSV tablets printed at: E) 16%; F) 20%, and G) 25% laser intensities.

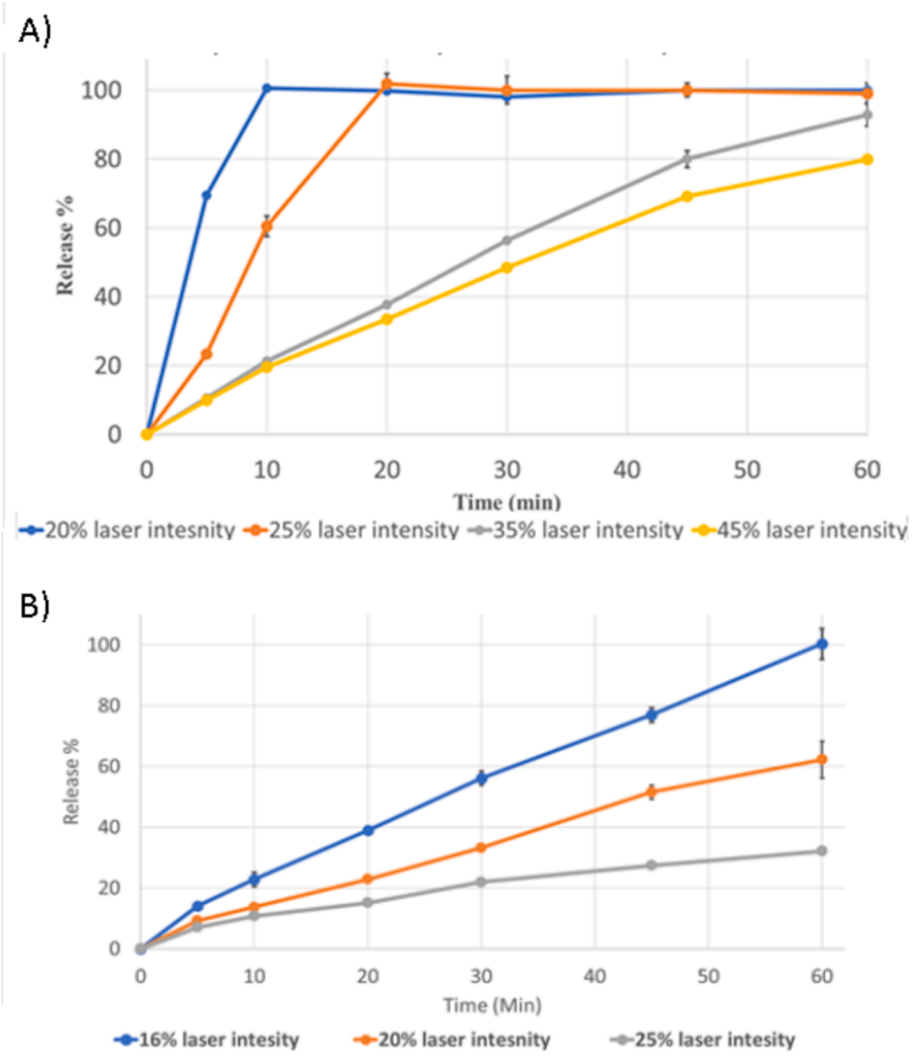

Fig. 9. *In vitro* drug release of monolithic 3D-printed tablets produced at various laser intensities. A) AAS tablets in citrate buffer pH 4.5 (n = 3). B) RSV tablets in citrate buffer pH 6.6 (n = 3).

influencing the uniform deposition of a thin, compact, and smooth layer of powder across the build area, which is essential for successful printing (Goodridge et al., 2012). Therefore, the size, distribution, and morphology of individual powder particles, were evaluated as these factors collectively impact powder flow. The results, depicted in Fig. 3, reveal that the average particle size (d50) of the VA64/AAS blend is 87.3 ± 0.61 μm, falling within the optimal range (45 to 90 μm) reported for SLS printing (Goodridge et al., 2006). Conversely, the HPMCAS-LMP/RSV blend exhibits an average particle size of 234.3 ± 1.15 μm. Although this value falls outside the specified range, literature suggests that this restriction may not always apply to pharmaceutical dosage forms as powders with particle sizes ranging from 150 to 350 μm can yield highly porous structures, which can be useful to achieve the desired disintegration and dissolution times (Tabriz et al., 2023). Both blends presented a monomodal particle size distribution with uniformity varying between 0.494 ± 0.003 (HPMCAS-LMP/RSV) and 0.675 ± 0.011 (AAS/VA64). Moreover, the SEM images revealed particles with spherical morphology for VA64/AAS blend and elliptical shape (oval and elongated features) for HPMCAS-LMP/RSV. Ultimately, the flowability of the blends was determined using the Carr's Index, and according to the results (VA64/AAS = 13.50 %; HPMCAS-LMP/RSV = 14.29 %) the powders are classified as presenting good flowability (11.0–15.0 %) (Goyal et al., 2015).

3.4. SLS for 3D printing of tablets

3.4.1. Production of monolithic tablets

The SLS printer consists of the printing chamber and powder reservoir which during the printing are heated to a temperature just under the melting point or the glass transition of the employed material. The SLS process begins with filling the building platform, which is set in the highest position, and reservoir chamber with the selected powder. The roller/blade is responsible for levelling a uniform and smooth layer of powder through several horizontal movements. Next, a high-power laser beam is emitted on to the top surface layer of powder and begins to sinter a pre-determined 2D pattern according to the 3D design. After each layer is completed, another thin layer of powder is dispersed. For that the printing chamber is lowered while the reservoir chamber is raised, which then allows the roller to apply a fresh powder surface on top of the completed layer. This process is repeated until the final layer is printed. After printing is complete, the sintered object which is contained in a powder cake within the printing chamber is extracted by shaking and sieving off the excess powder.

In this work, monolithic tablets were printed for each formulation using various laser intensities (Fig. 4). The objective was to initially optimize the parameters and then, based on the results, select the best condition for printing the bilayer tablet. A CO_2 laser (λ = 10.6 μm) was employed as the high-power laser beam, offering a significant advantage

Fig. 10. Tablet produced with the mesh design.

compared to other laser sources as it eliminates the need for incorporating an absorbance enhancer. This is because many biocompatible and biodegradable polymers absorb within the wavelength region of the CO_2 laser (Gueche et al., 2021). In contrast, in numerous reported SLS studies, Candurin was added to enhance absorbance and facilitate the sintering process for the production of pharmaceutical dosage forms (Barakh Ali et al., 2019; Hamed et al., 2021; Giri and Maniruzzaman, 2022).

Energy density (ED) is a crucial parameter in SLS printing, defined as the amount of energy transmitted per unit volume. It is determined by laser power, scanning speed, and layer thickness (Madžarević et al., 2021). For the initial experimentation, the scanning speed and layer thickness was kept constant for each formulation to isolate the influence of laser power.

These parameters were chosen through a trial-and-error approach (data not shown). Conversely, the laser power varied between 20 to 45 % for the AAS formulation, and 16 to 25 % for the RSV blend, producing tablets denoted as AAS20, AAS25, AAS35, AAS45, RSV16, RSV20, and RSV25, reflecting varying laser intensities.

The environment temperature was set at 60 and 90 °C for the AAS and RSV respectively. with the glass transition temperature (Tg) and degradation temperatures serving as key indicators for initial settings. Ideally, the temperature should be maintained near Tg to activate stress relaxation, which helps reduce part warpage and curling. However, it should not exceed Tg, as this would cause powder particles to stick together, complicating powder distribution (Yan et al., 2011). This optimal temperature is influenced by various factors, including the specific printer and laser type used, the chosen parameters, and whether the powder is fresh or reused.

As shown in Fig. 4, the AAS tablets appeared whitish and a slight change in colour and surface can be observed with increasing laser intensity, with AAS45 showing a light yellowish colour with compact surface. However, for RSV tablets, a significant alteration was evident with the increase of laser power, transitioning from slightly yellowish for RSV16 to a brownish core for RSV25. It worth mentioning that the colour change was also observed for the placebo tablets owing to HPMCAS-LMP properties and no RSV degradation was observed. Similar HPMCAS-LPM colour changes have been observed in previous studies (Scoutaris et al., 2018; Maniruzzaman et al., 2016).

3.4.2. Physical characterization of the monolithic tablets

As depicted in Table 2, augmenting the laser intensity resulted in increased hardness and reduced friability for both formulations. At lower laser intensities (AAS20 and RSV16), the hardness was relatively low for immediate-release tablets. However, by increasing the laser power, it became feasible to enhance the hardness. The friability of the tablets, in turn, exhibited an inversely proportional relationship to the laser intensity, decreasing as the laser power increased. For the AAS formulation, the lowest intensities (20/25) yielded highly friable tablets, whereas those produced with the highest intensities (35/45) remained within the specification (weight loss $\leq$ 1 %, (United States Pharmacopeia, 2018) USP 2018). In the case of RSV, despite the significant reduction in friability with the increase in laser power, the tablets did not meet the specification.

The hardness of SLS tablets reported in literature are variable depending on the excipients and parameters used (Brambilla et al., 2021). Some studies report low hardness values in the range of 14–18 N (Allahham et al., 2020), while others have achieved much higher breaking forces, reaching up to 280 N (Fina et al., 2018). Gueche et al (2021) reported hardness values similar to those found in the present study for VA64 tablets loaded with different concentrations of paracetamol (0–30 %), with results ranging from 89.32 N to 47.18 N when using 25 % laser power and a scan spacing of 25,000 pps (Gueche et al., 2021). A similar trend is observed with friability, where some studies meet the pharmacopoeia specification (<1% mass loss) (Tikhomirov et al., 2023; Fina et al., 2017), while others report highly friable tablets with mass losses between 24–30 % (Mitrousi, 2022).

3.4.3. 3D printing of bilayer tablets

The fabrication of the bilayer tablets was conducted subsequent to the optimization of printing and the production of monolithic tablets. Initially, the method involved: i) loading the first blend into the printer; ii) completing the printing process; iii) removing the first blend, while leaving the first layer of the tablet on the building platform; iv) adding the second blend to the printer; and v) reprinting onto the printed tablet. However, this approach was unsuccessful, as the tablet layers were not aligned (Fig. 5A).

To address this issue, a new method was developed wherein a 3D-printed casing was employed to maintain the compartments of the bilayer tablet in the correct position during the printing process. Fig. 5B outlines the procedure: i) one compartment of the tablet is printed; ii) the powder and the printed layer are removed from the print bed; iii) the casing is placed into the printer, and the first compartment is inserted into the casing slots; iv) new powder is loaded into the printer, and the second compartment is printed on top of the first one; and v) once the printing is completed, the bilayer tablets are removed from the casing. Using this technique, it is possible to produce bilayer tablets that are completely aligned (Fig. 5C). The tablets shown in Fig. 5 are for illustration purposes only and were manufactured using HPMCAS with 2 % food colouring to facilitate observation.

This new method was employed to fabricate bilayer tablets intended for the treatment of cardiovascular conditions. Initially, the RSV/HPMCAS-LMP compartment was printed, followed by the printing of the second layer containing the VA64/AAS formulation using the casing.

Fig. 6 depicts that, as expected, the first layer of RSV demonstrated a yellowish colour, while the second layer of AAS presented a whitish colour, similar to the results obtained for the monolithic tablets. Table 3 demonstrates the results for friability, hardness, and weight variation for

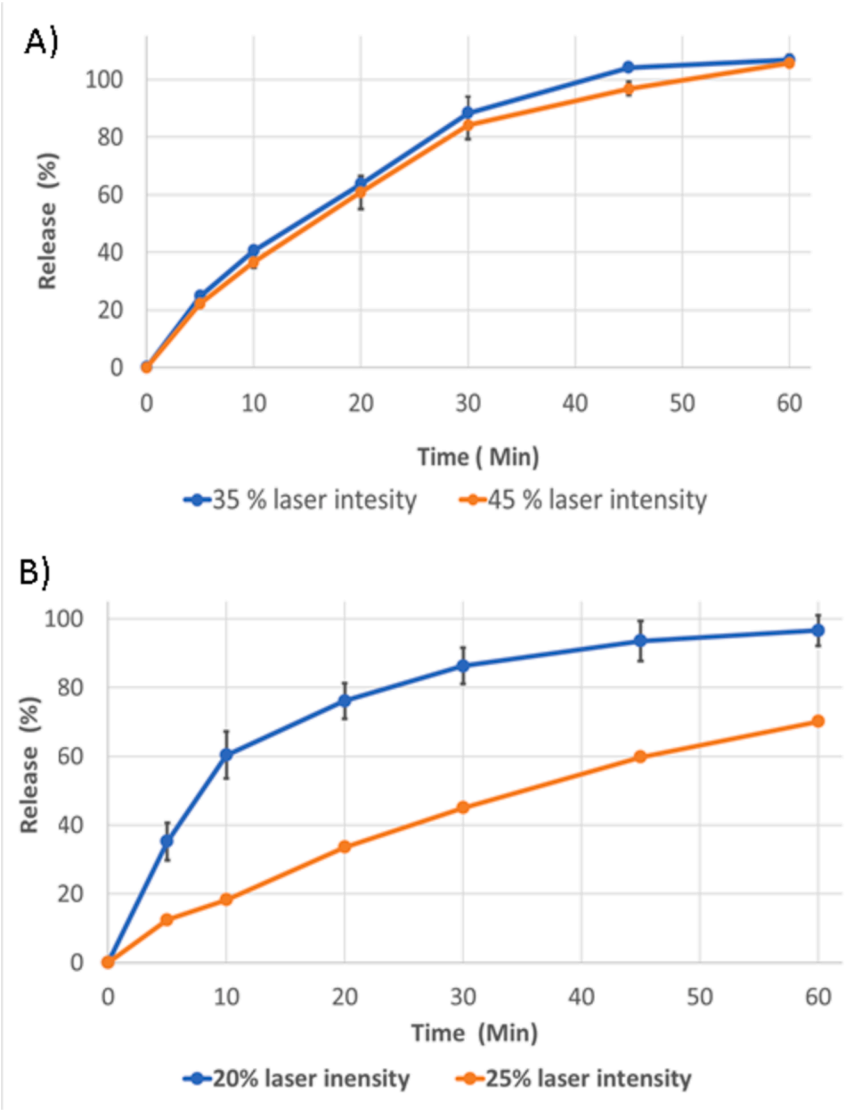

Fig. 11. *In vitro* drug release of mesh 3D-printed tablets produced at various laser intensities. A) AAS tablets in citrate buffer pH 4.5 (n = 3). B) RSV tablets in in citrate buffer pH 6.6 (n = 3).

the bilayer tablets, which are aligned with the values obtained for the monolithic tablets.

3.5. X-ray powder diffraction

XRPD analysis was conducted on bulk materials, PMs, and all tablets to identify the physical state of the APIs in the formulations. As depicted in Fig. 7A, VA64 displayed no peaks due to its amorphous nature, while the bulk AAS exhibited multiple sharp intensity peaks, indicating its crystalline state. AAS PM and tablets showed identical peaks at lower intensity, suggesting no alteration of AAS crystallinity. Although SLS has been reported as a technology capable of transforming drugs from a crystalline to an amorphous state (Thakkar et al., 2021), this was not an objective of this study, as AAS is classified as a BCS Class I drug and does not exhibit solubility issues (Dressman et al., 2012). As shown in Fig. 7B, HMPCAS-LMP demonstrates amorphous state since halo patterns without diffraction peaks were obtained. Bulk RSV (Fig. 7B) displayed a minor diffraction peak at 3.89°/2θ° and a broad peak at 19.50°/2θ°, indicating that the RSV used was in crystalline form C, which typically presents characteristic peaks at 3.6° + 2° and a broad peak at 19° + 5° (Blatter et al., 2006). A complete disappearance of the RSV diffractogram peak at 3.89°/2θ° was observed for RSV PM and tablets, possibly indicating the transformation of the drug into an amorphous state.

3.6. Scanning electron Microscopy (SEM)

The observation of the cross-sections of the 3D-printed tablets under SEM (Fig. 8) enabled the evaluation of their internal microstructures. As depicted in Fig. 8, in the case of AAS tablets, the inner cores became denser with the increase in laser intensity and consequently the sintering process. The AAS tablets produced with 20 % and 25 % laser intensity demonstrated a porous structure, while those produced with 35 % and 45 % showed completely molten particles, with the tablet cores appearing fused. Some voids can be observed in the AAS35 tablets, whereas they have virtually disappeared in the AAS45 tablets. Leong et al. (2001) also found that higher laser power led to narrower internal channels, and they established a linear correlation between porosity and laser power (Leong et al., 2001). A similar effect occurred for RSV tablets, where RSV16 exhibited a highly porous structure, RSV20 showed particles starting to melt, and finally, RSV25 resulted in a compact, non-porous structure.

In general, the porosity of RSV tablets was higher compared to AAS tablets, which could be attributed to the lower laser intensity used, as well as to the larger particle size previously described for the HPMCAS-

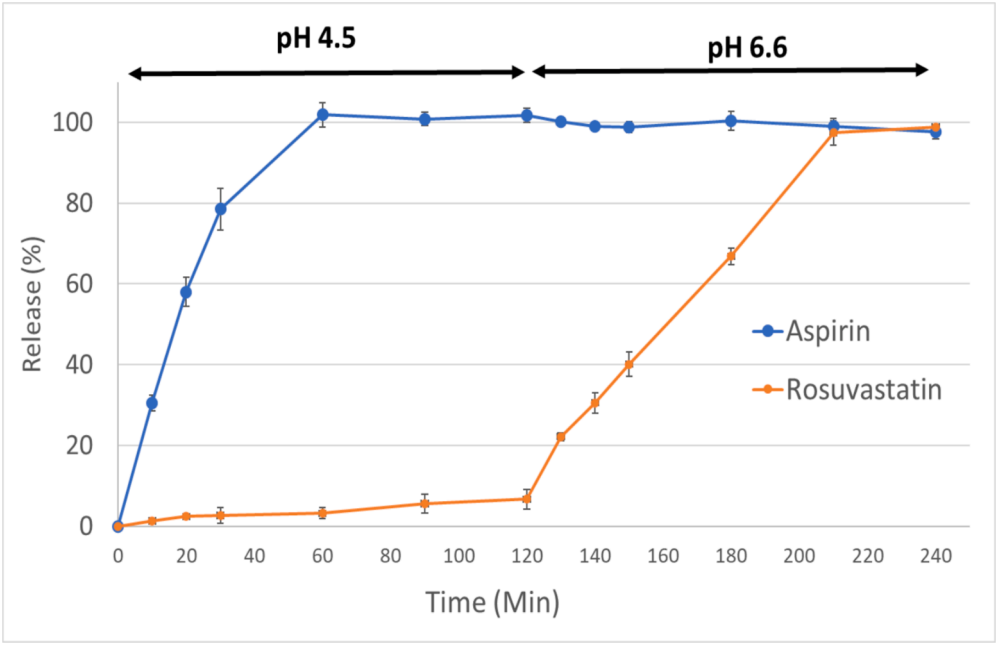

Fig. 12. *In vitro* drug release of bilayer 3D-printed tablets containing AAS and RSV evaluated 1 h at citrate buffer pH 4.5 (n = 3), followed by 1 h in pH 6.6 (n = 3).

LMP/RSV blend. This was attributed to the presence of larger particles in the HPMCAS-LMP/RSV blend were (d90) was found to be 453.7 μm and for the AA/VA64 much smaller at 209.7 μm respectively. Eventually as the laser intensity increased especially from 35-45 % the effect of larger particles in the blend (d90) was insignificant. Prior studies have demonstrated that finer particles (106–150 μm) increase the surface contact area, leading to a higher degree of sintering and therefore reduced porosity (Gueche et al., 2021; Salmoria et al., 2009).

3.7. *In vitro dissolution*

The in vitro dissolution of the 3D-printed monolithic tablets produced at various laser intensities was evaluated. Fig. 9 illustrates that increasing the laser intensity led to a reduction in the dissolution rates of both AAS and RSV tablets. AAS tablets printed at laser intensities of 20 and 25 % achieved approximately 100 % API dissolution within 30 min, aligning with USP specifications (80 % of AAS dissolved in 30 min). On the other hand, those fabricated at 35 and 45 % of laser power showed a release outside the specification, ranging around 48–56 % within the same timeframe. A similar trend was observed for RSV tablets, with releases of approximately 20 %, 31 %, and 58 % at 30 min for tablets fabricated at 25 %, 20 %, and 16 % laser power, respectively. According to USP, 75 % of RSV should dissolve within 30 min.

As tablets with the highest dissolution rates exhibited poor physical properties (hardness and friability) due to low laser intensity, the focus shifted to tablets produced with the highest laser power. However, their drug release did not align with specifications. To enhance the dissolution rate of these tablets, fabrication dosage forms with a mesh design was explored (Fig. 10). The aim was to create a design with a higher surface area to volume (SA/V) ratio, as studies have shown that API release is faster with a higher SA/V ratio and slower with a smaller ratio (Reynolds et al., 2002; Narayana Raju et al., 2010; Windolf et al., 2021). Consequently, AAS and RSV mesh tablets were printed using the same formulation and parameters as the solid tablets, at laser intensities of 35/45 % and 20/25 %, respectively.

Fig. 11 illustrates the in vitro release of the mesh tablets, revealing that the new design effectively enhanced the dissolution rate of both AAS and RSV tablets. In comparison to solid tablets, the dissolution of AAS mesh tablets increased from 56 % to 90 % for AAS35 and from 48 % to 85 % for AAS45, ensuring compliance with USP specifications. Similarly, RSV mesh tablets exhibited a marked increase in dissolution rate from 31 % to 87 % for RSV20 and from 20 % to 45 % for RSV25. Consequently, RSV20 met pharmacopeial specifications.

Considering the results for the monolithic tablets, the AAS mesh tablets manufactured at 45 % laser power were chosen as one compartment of the ultimate bilayer tablet. While the reasonable option for the RSV compartment would be the 20 % mesh tablet, we opted for the solid tablet instead. This decision was made to assess the influence of a solid layer on the dissolution of the bilayer system.

As Fig. 12 demonstrates, for the bilayer tablet, around 80 % of AAS was released in 30 min, which is close to the value found for the monolithic tablet (85 %). As expected, RSV showed minimal release in the pH 4.5 environment due to its pH-dependent solubility behaviour, attributed to the ionization of the carboxylic acid group (pKa = 4.6) at higher pH levels. After 120 min, the pH was adjusted to 6.6, then after 30 min (150 min), RSV tablet showed a release of 40 % of API, slightly higher compared to the monolithic tablets (31 %). Overall, the impact on dissolution was minor when the two compartments were printed together in a single tablet.

4. Conclusion

SLS was employed in this work to produce bilayer tablets for the treatment of heart conditions. The careful choice of the AAS/VA64 and RSV/HPMCAS-LMP powder blends, tablet design and the tuning of print processing parameters led to the fabrication of monolithic and bilayer tablets. The laser intensity was crucial for the print process optimisation and affected the tablet hardness, friability, and drug dissolution rates. The printing of robust bilayer tablets with specific designs demonstrated the suitability of SLS technology for polypills. Moreover, SLS was proved to produce tablets with high reproducibility and accuracy with fewer processing steps showing the immense potential for the manufacturing of pharmaceutical drug products both at the point of care of mass production. Some minor issues related to powder de-dusting, and occupational health risks require further investigation.

CRediT authorship contribution statement

Laura Andrade Junqueira: Writing – review & editing, Writing – original draft, Validation, Methodology, Investigation, Formal analysis, Data curation. **Atabak Ghanizadeh Tabriz:** Writing – original draft, Validation, Methodology, Investigation, Formal analysis, Data curation. **Vivek Garg:** Validation, Resources, Methodology, Formal analysis, Data curation. **Siva Satyanarayana Kolipaka:** Validation, Methodology, Investigation, Formal analysis, Data curation. **Ho-Wah Hui:** Visualization, Supervision, Resources, Project administration, Methodology, Investigation, Funding acquisition, Conceptualization. **Nathan Boersen:** Writing – original draft, Visualization, Validation, Supervision, Methodology, Investigation, Funding acquisition, Data curation, Conceptualization. **Sandra Roberts:** Visualization, Supervision, Resources, Project administration, Methodology, Funding acquisition, Conceptualization. **John Jones:** Writing – original draft, Visualization, Supervision, Resources, Project administration, Methodology, Funding acquisition. **Dennis Douroumis:** Writing – review & editing, Writing – original draft, Visualization, Supervision, Resources, Project administration, Investigation, Funding acquisition, Formal analysis, Data curation, Conceptualization.

Declaration of competing interest

The authors declare that they have no known competing financial interests or personal relationships that could have appeared to influence the work reported in this paper.

Data availability

Data will be made available on request.

References

Abdella, S., Youssef, S.H., Afinjuomo, F., Song, Y., Fouladian, P., Upton, R., Garg, S., 2021. 3D Printing of Thermo-Sensitive Drugs. Pharmaceutics 13 (9), 1524. https://doi.org/10.3390/pharmaceutics13091524.

Allahham, N., Fina, F., Marcuta, C., Kraschew, L., Mohr, W., Gaisford, S., Basit, A.W., Goyanes, A., 2020. Selective Laser Sintering 3D Printing of Orally Disintegrating Printlets Containing Ondansetron. Pharmaceutics 12 (2), 110. https://doi.org/10.3390/pharmaceutics12020110.

Alonzo, M., Khoury, R.E., Nagiah, N., Thakur, V., Chattopadhyay, M., Joddar, B., 2022. 3D biofabrication of a cardiac tissue construct for sustained longevity and function. ACS Appl. Mater. Interfaces 14 (19), 21800–21813. https://doi.org/10.1021/acsami.1c23883.

Alzahrani, A., Narala, S., Youssef, A.A.A., Nyavanandi, D., Bandari, S., Mandati, P., Almotairy, A., Almutairi, M., Repka, M., 2022. Fabrication of a shell-core fixed-dose combination tablet using fused deposition modeling 3D printing. Eur. J. Pharm. Biopharm. 177, 211–223. https://doi.org/10.1016/j.ejpb.2022.07.003.

Araújo, M., Sa-Barreto, L., Gratieri, T., Gelfuso, G., Cunha-Filho, M., 2019. The Digital Pharmacies Era: How 3D printing technology using fused deposition modeling can Become a Reality. Pharmaceutics 11 (3), 128. https://doi.org/10.3390/pharmaceutics11030128.

Arnett, D.K., Blumenthal, R.S., Albert, M.A., Buroker, A.B., Goldberger, Z.D., Hahn, E.J., Himmelfarb, C.D., Khera, A., Lloyd-Jones, D., McEvoy, J.W., Michos, E.D., Miedema, M.D., Muñoz, D., Smith, S.C., Virani, S.S., Williams, K.A., Yeboah, J., Ziaeian, B., 2019. 2019 ACC/AHA Guideline on the Primary Prevention of Cardiovascular Disease: A Report of the American College of Cardiology/American Heart Association Task Force on Clinical Practice Guidelines. Circulation 140 (11), e596–e646. https://doi.org/10.1161/CIR.0000000000000678.

Awad, A., Fina, F., Trenfield, S.J., Patel, P., Goyanes, Á.G., Gaisford, S., Basit, A.W., 2019. 3D Printed Pellets (MiniPrintlets): a novel, Multi-Drug, controlled release platform technology. Pharmaceutics 11 (4), 148. https://doi.org/10.3390/pharmaceutics11040148.

Barakh Ali, S.F., Mohamed, E.M., Ozkan, T., Kuttolamadom, M.A., Khan, M.A., Asadi, A., Rahman, Z., 2019. Understanding the effects of formulation and process variables on the printlets quality manufactured by selective laser sintering 3D printing. Int. J. Pharm. 570, 118651. https://doi.org/10.1016/j.ijpharm.2019.118651.

Beer, N., Hegger, I., Kaae, S., De Bruin, M.L., Genina, N., Alves, T.L., Hoebert, J., Sporrong, S.K., 2021. Scenarios for 3D printing of personalized medicines - A case study. Exploratory Research in Clinical and Social Pharmacy 4, 100073. https://doi.org/10.1016/j.rcsop.2021.100073.

Blatter, F., Schaaf, P.A.V.D., Szelagiewicz, M., 2006. Crystalline forms of rosuvastatin calcium salt. Accessed 15th Apr 2024 Available Online. https://patentimages.storage.googleapis.com/6a/79/4f/8154bdfa446548/WO2006079611A1.pdf.

Brambilla, C.R., Okafor-Muo, O.L., Hassanin, H., ElShaer, A., 2021. 3DP Printing of Oral Solid Formulations: A Systematic Review. Pharmaceutics 13 (3), 358. https://doi.org/10.3390/pharmaceutics13030358.

Cader, H.K., Rance, G.A., Alexander, M.R., Gonçalves, A.D., Roberts, C.J., Tuck, C.J., Wildman, R.D., 2019. Water-based 3D inkjet printing of an oral pharmaceutical dosage form. Int. J. Pharm. 564, 359–368. https://doi.org/10.1016/j.ijpharm.2019.04.026.

Charoo, N.A., Ali, S.F.B., Mohamed, E.M., Kuttolamadom, M.A., Ozkan, T., Khan, M.A., Rahman, Z., 2020. Selective laser sintering 3D printing – an overview of the technology and pharmaceutical applications. Drug Dev. Ind. Pharm. 46 (6), 869–877. https://doi.org/10.1080/03639045.2020.1764027.

Chou, R.; Cantor, A.; Dana, T.; Wagner, J.; Ahmed, A.; Fu, R.; Ferencik, M. Statin Use for the Primary Prevention of Cardiovascular Disease in Adults: A Systematic Review for the U.S. Preventive Services Task Force. Rockville (MD): Agency for Healthcare Research and Quality (US); 2022. (Evidence Synthesis, No. 219.) Available from: https://www.ncbi.nlm.nih.gov/books/NBK583661/.

Davis, D.A., Thakkar, R., Su, Y., Williams, R.O., Maniruzzaman, M., 2021. Selective laser sintering 3-Dimensional printing as a single step process to prepare amorphous solid dispersion dosage forms for improved solubility and dissolution rate. J. Pharm. Sci. 110 (4), 1432–1443. https://doi.org/10.1016/j.xphs.2020.11.012.

Dressman, J.B., Nair, A., Abrahamsson, B., Barends, D.M., Groot, D.W., Kopp, S., Langguth, P., Polli, J.E., Shah, V.P., Zimmer, M., 2012. Biowaiver Monograph for Immediate-Release Solid oral dosage forms: acetylsalicylic acid. J. Pharm. Sci. 101 (8), 2653–2667. https://doi.org/10.1002/jps.23212.

Eleftheriadis, G.K., Kantarelis, E., Monou, P.K., Andriotis, E.G., Bouropoulos, N., Tzimtzimis, E.K., Tzetzis, D., Rantanen, J., Fatouros, D.G., 2021. Automated digital design for 3D-printed individualized therapies. Int. J. Pharm. 599, 120437. https://doi.org/10.1016/j.ijpharm.2021.120437.

Fina, F., Goyanes, A., Gaisford, S., Basit, A.W., 2017. Selective laser sintering (SLS) 3D printing of medicines. Int. J. Pharm. 529 (1–2), 285–293. https://doi.org/10.1016/j.ijpharm.2017.06.082.

Fina, F., Goyanes, A., Madla, C.M., Awad, A., Trenfield, S.J., Kuek, J.M., Patel, P., Gaisford, S., Basit, A.W., 2018. 3D printing of drug-loaded gyroid lattices using selective laser sintering. Int. J. Pharm. 547 (1–2), 44–52. https://doi.org/10.1016/j.ijpharm.2018.05.044.

Fina, F., Madla, C.M., Goyanes, A., Zhang, J., Gaisford, S., Basit, A.W., 2018. Fabricating 3D printed orally disintegrating printlets using selective laser sintering. Int. J. Pharm. 541 (1–2), 101–107. https://doi.org/10.1016/j.ijpharm.2018.02.015.

Fu, J., Yu, X., Jin, Y., 2018. 3D printing of vaginal rings with personalized shapes for controlled release of progesterone. Int. J. Pharm. 539 (1–2), 75–82. https://doi.org/10.1016/j.ijpharm.2018.01.036.

Giri, B.R., Maniruzzaman, M., 2022. Fabrication of Sustained-Release dosages using Powder-Based Three-Dimensional (3D) printing technology. AAPS PharmSciTech 24 (1). https://doi.org/10.1208/s12249-022-02461-z.

Goodridge, R.D., Dalgarno, K.W., Wood, D.J., 2006. Indirect selective laser sintering of an apatite-mullite glass-ceramic for potential use in bone replacement applications. Proc. Inst. Mech. Eng. [H] 220 (1), 57–68. https://doi.org/10.1243/095441105x69051.

Goodridge, R.D., Tuck, C.J., Hague, R.J.M., 2012. Laser sintering of polyamides and other polymers. Prog. Mater Sci. 57 (2), 229–267. https://doi.org/10.1016/j.pmatsci.2011.04.001.

Goyal, A., Sharma, V., Sihag, M.K., Tomar, S.K., Arora, S., Sabikhi, L., Singh, A.K., 2015. Development and physico-chemical characterization of microencapsulated flaxseed oil powder: A functional ingredient for omega-3 fortification. Powder Technol. 286, 527–537. https://doi.org/10.1016/j.powtec.2015.08.050.

Gueche, Y.A., Sanchez-Ballester, N.M., Cailleaux, S., Bataille, B., Soulairol, I., 2021. Selective Laser Sintering (SLS), a New Chapter in the Production of Solid Oral Forms (SOFs) by 3D Printing. Pharmaceutics 13, 1212. https://doi.org/10.3390/pharmaceutics13081212.

Gueche, Y.A., Sanchez-Ballester, N.M., Bataille, B., Aubert, A., Leclercq, L., Rossi, J.-C., Soulairol, I., 2021. Selective Laser Sintering of Solid Oral Dosage Forms with Copovidone and Paracetamol Using a CO2 Laser. Pharmaceutics 13 (2), 160. https://doi.org/10.3390/pharmaceutics13020160.

Hamed, R., Mohamed, E.M., Rahman, Z., Khan, M.A., 2021. 3D-printing of lopinavir printlets by selective laser sintering and quantification of crystalline fraction by XRPD-chemometric models. Int. J. Pharm. 592, 120059. https://doi.org/10.1016/j.ijpharm.2020.120059.

He, Y., Luckett, J., Begines, B., Dubern, J.-F., Hook, A.L., Prina, E., Rose, F.R.A.J., Tuck, C.J., Hague, R.J.M., Irvine, D.J., Williams, P., Alexander, M.R., Wildman, R.D., 2022. Ink-jet 3D printing as a strategy for developing bespoke non-eluting biofilm resistant medical devices. Biomaterials 281, 121350. https://doi.org/10.1016/j.biomaterials.2021.121350.

Jakus, A. E. An Introduction to 3D Printing—Past, present, and Future promise. 3D Printing In Orthopaedic Surgery, 2019; pp. 1-15, 2019. https://doi.org/10.1016/b978-0-323-58118-9.00001-4.

Junqueira, L.A., Tabriz, A.G., Raposo, F.J., Carobini, L.R., Vaz, U.P., Brandão, M.A.F., Douroumis, D., Raposo, N.R.B., 2022. Coupling of fused deposition modeling and inkjet printing to produce drug loaded 3D printed tablets. Pharmaceutics 14 (1), 159. https://doi.org/10.3390/pharmaceutics14010159.

Karakurt, I., Aydoğdu, A., Çıkrıkcı, S., Orozco, J., Lin, L., 2020. Stereolithography (SLA) 3D printing of ascorbic acid loaded hydrogels: A controlled release study. Int. J. Pharm. 584, 119428. https://doi.org/10.1016/j.ijpharm.2020.119428.

Khaled, S.A., Burley, J.C., Alexander, M.R., Yang, J., Roberts, C.J., 2015. 3D printing of five-in-one dose combination polypill with defined immediate and sustained release profiles. J. Control. Release 217, 308–314. https://doi.org/10.1016/j.jconrel.2015.09.028.

Kulinowski, P., Malczewski, P., Łaszcz, M., Baran, E., Milanowski, B., Kuprianowicz, M., Dorożyński, P., 2022. Development of composite, Reinforced, Highly Drug-Loaded pharmaceutical printlets manufactured by Selective Laser Sintering—In search of relevant excipients for pharmaceutical 3D printing. Materials 15 (6), 2142. https://doi.org/10.3390/ma15062142.

Leong, K.F., Phua, K.K.S., Chua, C.K., Du, Z.H., Teo, K.O.M., 2001. Fabrication of porous polymeric matrix drug delivery devices using the selective laser sintering technique. Proc. Inst. Mech. Eng. [H] 215 (2), 191–192. https://doi.org/10.1243/0954411011533751.

Leong, K.F., Chua, C.K., Gui, W.S., Verani, N., 2006. Building porous biopolymeric microstructures for controlled drug delivery devices using selective laser sintering. Int. J. Adv. Manuf. Technol. 31 (5–6), 483–489. https://doi.org/10.1007/s00170-005-0217-4.

Liu, J., Tagami, T., Ozeki, T., 2020. Fabrication of 3D-Printed Fish-Gelatin-Based polymer hydrogel patches for local delivery of PEGylated liposomal doxorubicin. Mar. Drugs 18 (6), 325. https://doi.org/10.3390/md18060325.

Madžarević, M., Medarević, D., Pavlović, S., Ivković, B., Đuriš, J., Ibrić, S., 2021. Understanding the effect of energy density and formulation factors on the printability and characteristics of SLS Irbesartan Tablets—Application of the Decision Tree Model. Pharmaceutics 13 (11), 1969. https://doi.org/10.3390/pharmaceutics13111969.

Mallon, A., Farnan, T., 2021. A case report detailing the use of 3D printing technology in surgical planning and decision making in ENT surgery-an axial 3D first in Northern Ireland. Int. J. Surg. Case Rep. 87, 106407. https://doi.org/10.1016/j.ijscr.2021.106407.

Maniruzzaman, M., Islam, M.T., Halsey, S., Amin, D., Douroumis, D., 2016. Novel Controlled Release Polymer-Lipid Formulations Processed by Hot Melt Extrusion. AAPS PharmSciTech 17 (1), 191–199. https://doi.org/10.1208/s12249-015-0470-2.

Melocchi, A., Uboldi, M., Briatico-Vangosa, F., Moutaharrik, S., Cerea, M., Foppoli, A., Maroni, A., Palugan, L., Zema, L., Gazzaniga, A., 2021. The ChronotopicTM system for pulsatile and colonic delivery of active molecules in the era of precision Medicine: Feasibility by 3D printing via fused Deposition Modeling (FDM). Pharmaceutics 13 (5), 759. https://doi.org/10.3390/pharmaceutics13050759.

Mitrousi, Marina-Eirini, Investigation of laser sintering of pharmaceutical excipients for oral solid dosage forms. 2022, PhD thesis, University of Nottingham. Available at: https://eprints.nottingham.ac.uk/68693/.

Mohamed, E.M., Ali, S.F.B., Rahman, Z., Dharani, S., Ozkan, T., Kuttolamadom, M.A., Khan, M.A., 2020. Formulation Optimization of selective laser sintering 3D-Printed tablets of Clindamycin palmitate hydrochloride by response surface methodology. AAPS PharmSciTech 21 (6). https://doi.org/10.1208/s12249-020-01775-0.

Narayana Raju, P., Prakash, K., Rama Rao, T., Reddy, B.C.S., Sreenivasulu, V., Lakshmi Narasu, M., 2010. Effect of Tablet Surface Area and Surface Area/Volume on Drug Release from Lamivudine Extended Release Matrix Tablets. Int. J. Pharmaceut. Sci. Nanotechnol. 3 (1), 872–876. https://doi.org/10.37285/ijpsn.2010.3.1.11.

Osouli-Bostanabad, K., Adibkia, K., 2018. Made-on-demand, complex and personalized 3D-printed drug products. Bioimpacts 8 (2), 77–79. https://doi.org/10.15171/bi.2018.09.

Patel, S.K., Khoder, M., Peak, M., Alhnan, M.A., 2021. Controlling drug release with additive manufacturing-based solutions. Adv. Drug Deliv. Rev. 174, 369–386. https://doi.org/10.1016/j.addr.2021.04.020.

Pereira, G.G., Figueiredo, S., Fernandes, A.I., Pinto, J.F., 2020. Polymer selection for Hot-Melt extrusion coupled to fused deposition modelling in pharmaceutics. Pharmaceutics 12 (9), 795. https://doi.org/10.3390/pharmaceutics12090795.

Reynolds, T.D., Mitchell, S.A., Balwinski, K.M., 2002. Investigation of the Effect of Tablet Surface Area/Volume on Drug Release from Hydroxypropylmethylcellulose Controlled-Release Matrix Tablets. Drug Dev. Ind. Pharm. 28 (4), 457–466. https://doi.org/10.1081/ddc-120003007.

Robles-Martinez, P., Xu, X., Trenfield, S.J., Awad, A., Goyanes, A., Telford, R., Basit, A. W., Gaisford, S., 2019. 3D printing of a Multi-Layered polypill containing six drugs using a novel stereolithographic method. Pharmaceutics 11 (6), 274. https://doi.org/10.3390/pharmaceutics11060274.

Salmoria, G.V., Klauss, P., Paggi, R.A., Kanis, L.A., Lago, A., 2009. Structure and mechanical properties of cellulose based scaffolds fabricated by selective laser sintering. Polym. Test. 28 (6), 648–652. https://doi.org/10.1016/j.polymertesting.2009.05.008.

Salmoria, G.V., Klauss, P., Zepon, K.M., Kanis, L.A., 2013. The effects of laser energy density and particle size in the selective laser sintering of polycaprolactone/progesterone specimens: morphology and drug release. Int. J. Adv. Manuf. Technol. 66 (5–8), 1113–1118. https://doi.org/10.1007/s00170-012-4393-8.

Sandler, N., Preis, M., 2016. Printed Drug-Delivery Systems for improved patient treatment. Trends Pharmacol. Sci. 37 (12), 1070–1080. https://doi.org/10.1016/j.tips.2016.10.002.

Scoutaris, N., Ross, S.A., Douroumis, D., 2018. 3D printed "Starmix" drug loaded dosage forms for paediatric applications. Pharm. Res. 35 (2). https://doi.org/10.1007/s11095-017-2284-2.

Tabriz, A.G., Kuofie, H., Scoble, J., Boulton, S., Douroumis, D., 2023. Selective Laser Sintering for printing pharmaceutical dosage forms. J. Drug Delivery Sci. Technol. 86, 104699. https://doi.org/10.1016/j.jddst.2023.104699.

Tabriz, A.G., Gonot-Munck, Q., Baudoux, A., Garg, V., Farnish, R., Katsamenis, O.L., Hui, H.-W., Boersen, N., Roberts, S., Jones, J., Douroumis, D., 2023. 3D printing of personalised carvedilol tablets using selective laser sintering. Pharmaceutics 15 (9), 2230. https://doi.org/10.3390/pharmaceutics15092230.

Tagami, T., Ito, E., Kida, R., Hirose, K., Noda, T., Ozeki, T., 2021. 3D printing of gummy drug formulations composed of gelatin and an HPMC-based hydrogel for pediatric use. Int. J. Pharm. 594, 120118. https://doi.org/10.1016/j.ijpharm.2020.120118.

Thakkar, R., Jara, M.O., Swinnea, S., Pillai, A.R., Maniruzzaman, M., 2021. Impact of laser speed and drug particle size on selective laser sintering 3D printing of amorphous solid dispersions. Pharmaceutics 13 (8), 1149. https://doi.org/10.3390/pharmaceutics13081149.

Tikhomirov, E., Åhlén, M., Di Gallo, N., Strømme, M., Kipping, T., Quodbach, J., Lindh, J., 2023. Selective laser sintering additive manufacturing of dosage forms: Effect of powder formulation and process parameters on the physical properties of printed tablets. Int. J. Pharm. 635, 122780. https://doi.org/10.1016/j.ijpharm.2023.122780.

Triacca, A., Pitzanti, G., Mathew, E., Conti, B., Dorati, R., Lamprou, D.A., 2022. Stereolithography 3D printed implants: A preliminary investigation as potential local drug delivery systems to the ear. Int. J. Pharm. 616, 121529. https://doi.org/10.1016/j.ijpharm.2022.121529.

Uddin, M.J., Scoutaris, N., Klepetsanis, P., Chowdhry, B., Prausnitz, M.R., Douroumis, D., 2015. Inkjet printing of transdermal microneedles for the delivery of anticancer agents. Int. J. Pharm. 494 (2), 593–602. https://doi.org/10.1016/j.ijpharm.2015.01.038.

2018. MD, USA.

Van Der Stelt, M.; Grobusch, Martin. P.; Koroma, Abdul. R.; Papenburg, M.; Kebbie, I.; Slump, Cornelis. H.; Maal, T. J. J.; Brouwers, L. Pioneering low-cost 3D-printed transtibial prosthetics to serve a rural population in Sierra Leone – an observational cohort study. EClinicalMedicine 2021, 35, 100874. https://doi.org/10.1016/j.eclinm.2021.100874.

Windolf, H., Chamberlain, R., Quodbach, J., 2021. Predicting Drug Release from 3D Printed Oral Medicines Based on the Surface Area to Volume Ratio of Tablet Geometry. Pharmaceutics 13 (9), 1453. https://doi.org/10.3390/pharmaceutics13091453.

Yan, T.-T., Lv, Z.-F., Tian, P., Lin, M.-M., Lin, W., Huang, S.-Y., Chen, Y.-Z., 2020. Semi-solid extrusion 3D printing ODFs: an individual drug delivery system for small scale pharmacy. Drug Dev. Ind. Pharm. 46 (4), 531–538. https://doi.org/10.1080/03639045.2020.1734018.

Yan, C., Shi, Y., Hao, L., 2011. Investigation into the Differences in the Selective Laser Sintering between Amorphous and Semi-crystalline Polymers. *Int. Polym. Proc.* 26 (4), 416–423. https://doi.org/10.3139/217.2452.

Youman, S., Dang, E., Jones, M., Duran, D., Brenseke, B., 2021. The Use of 3D Printers in Medical Education with a Focus on Bone Pathology. Medical Science Educator 31 (2), 581–588. https://doi.org/10.1007/s40670-021-01222-0.

Yusuf, S., Attaran, A., Bosch, J., Joseph, P., Lonn, E., McCready, T., Mente, A., Nieuwlaat, R., Pais, P., Rodgers, A., Schwalm, J.D., Smith, R., Teo, K., Xavier, D., 2014. Combination pharmacotherapy to prevent cardiovascular disease: present status and challenges. Eur. Heart J. 35 (6), 353–364. https://doi.org/10.1093/eurheartj/eht407.